Modulation of proximity to criticality enhances slow activity fluctuations during free recall

Yellin D[1]., Siegel N.[2], Malach R[1]., Shriki O.[2,3]

[1] Department of Brain Sciences, Weizmann Institute of Science, Rehovot, Israel

[2] Department of Computer Science, Ben-Gurion University of the Negev, Beer-Sheva, Israel

[3] Department of Cognitive and Brain Sciences, Ben-Gurion University of the Negev, Beer-Sheva, Israel

Abstract

Categorically bounded free recall allows generating perceptual and cognitive contents within specific categories while avoiding unrelated intrusions. Previous research suggested that this is implemented via amplification of ultra-slow spontaneous activity fluctuations, initiating a spontaneous recall event. However, the underlying amplification mechanism remains unclear. Here, we demonstrate, using a simulation of a simple random recurrent neuronal network operating near a critical point, that such selective amplification can be generated by a small shift towards this critical point, resulting in a dynamical phenomenon termed "critical slowing down". By fitting physiological parameters and applying stochastic white noise input, we simulated ultra-slow fluctuations observed during rest and categorically bounded visual recall in the human cortex. Our findings suggest that modulation of spontaneous fluctuations linked to free recall can be explained by a stochastically driven recurrent network near a critical point, providing insight into the rapid and flexible formation of categorical boundaries in human cognition.

Introduction

Human free behavior, a fundamental aspect of human nature, is less studied compared to stimulus-response behaviors. We previously proposed (Moutard et al., 2015; Norman et al., 2017) that ultra-slow spontaneous activity fluctuations , also known as “resting-state” activity (Raichle, 2011), drive free and creative behaviors in the human brain. The power spectrum of these fluctuations has been characterized as obeying a power-law profile (He, 2014; Miller et al., 2009; Nir et al., 2008) and they emerge in well-defined networks across the cortex, uncovering unique patterns of functional connectivity (Buzsáki, 2006; Fox & Raichle, 2007; Nir et al., 2006; Eldar et al., 2013; Gilaie-Dotan et al., 2013; Hahamy et al., 2015; Harmelech & Malach, 2013; Smith et al., 2015; Wilf et al., 2015). They have also been linked to other spontaneous physiological manifestations such as pupil diameter fluctuations (Yellin et al., 2015) and eye-drifts (Ramot et al., 2011). We recently demonstrated a direct link between the spontaneous activity fluctuations and free and creative verbal behaviors (Broday-Dvir & Malach, 2021).

Free behavior relies on the ability to rapidly and flexibly set boundaries for the behavior within specific domains. For instance, jazz musicians can restrict their improvisation to the music domain and specific scales, while dancers exert spontaneous behavior within the domain of motor movement and specific dancing styles. If the slow spontaneous fluctuations indeed underlie free behaviors, a mechanism must be present in the brain to regulate these fluctuations' boundaries. In a study exploring this idea in the domain of free visual imagery and recall, Norman et al. (2017) found that resting state fluctuations displayed an increase in baseline and power of the slow spontaneous fluctuations, specifically in neuronal groups representing the targeted categories. This local baseline shift was predicted to bring the targeted neurons closer to the decision threshold and enhance the probability of the free behaviors being expressed within the intended boundaries.

However, although these complex neuronal phenomena have been well characterized at high spatial and temporal precision, we are still in the dark as to the neuronal mechanisms that underlie them. Specifically, it is not clear how the characteristic power spectrum of the spontaneous fluctuations - dominated by ultra-slow frequencies - emerges out of the typically fast neuronal elements. Furthermore, the neuronal mechanism that drives the

baseline shift is unknown. So is the process driving selective slow-frequency amplifications that are observed in categorically targeted free behaviors.

Near-critical dynamics as a potential mechanism. Here, we rely on the hypothesis that the cortex operates near criticality (Beggs, 2022; Beggs & Plenz, 2003; Kinouchi & Copelli, 2006; Shew et al., 2009) and propose that the abovementioned phenomena can be explained in the context of a fundamental property of near-critical recurrent systems - the slowing down of stochastic fluctuations as these systems approach criticality. Termed "critical slowing down" (Lee et al., 2014; Meisel et al., 2015; Scheffer et al., 2009), the phenomenon describes the universal tendency of systems near a transition point in their dynamics to exhibit slower time scales and take longer time to relax to a steady state equilibrium following perturbations. The slowing down of spontaneous fluctuations near criticality can explain the unique power spectra of fluctuations observed in the resting state networks. Additionally, we suggest that the modulation of spontaneous fluctuations provides a mechanism for the efficient implementation of the boundary setting regulation required for free behaviors to operate within specific domains. By bringing targeted neurons closer to the decision threshold, the baseline spectral shift of the spontaneous fluctuations can enhance the probability of free behaviors being expressed within specific boundaries.

Recent experimental and theoretical evidence supports the idea that the healthy cortex operates near a critical point, exhibiting slow time scales and scale-free dynamics (Arviv et al., 2015; Deco & Jirsa, 2012; Haimovici et al., 2013; Linkenkaer-Hansen et al., 2001; Shew & Plenz, 2013; Shriki et al., 2013; Yu et al., 2013). Scale-free spatiotemporal cascades of neuronal activity, termed neuronal avalanches, have been found in *in vitro* and *in vivo* animal studies as well as in large-scale human fMRI, EEG and MEG recordings (Arviv et al., 2015; Lombardi et al., 2021; Palva et al., 2013; Tagliazucchi et al., 2012). These avalanches can be well described by the framework of critical branching processes (Harris, 2012). Other studies indicated edge-of-chaos criticality (Bertschinger & Natschläger, 2004; Legenstein & Maass, 2007; Toker et al., 2022). Importantly, near-critical dynamics optimize information processing (Shew et al., 2009; Shriki & Yellin, 2016) and deviations from critical dynamics are associated with disorders in information processing (Arviv et al., 2016; Dotan & Shriki, 2021; Fekete et al., 2018, 2021). We have previously demonstrated the phenomenon of critical slowing down (CSD) in a recurrent network model of early visual processing, where the

effective time scales grow longer as the network approaches a critical point during its learning process (Shriki & Yellin, 2016). For a recent review of critical brain dynamics, see (Beggs, 2022; O'Byrne & Jerbi, 2022).

Network model and tuning of proximity to criticality. To explore the suggested mechanism, we simulated a recurrent network of rate-based units at varying proximities to criticality. These rate models can be rigorously derived from large-scale conductance-based networks that model cortical dynamics (Shriki et al., 2003). Our network architecture is adapted from the one proposed by Chaudhuri et al. (2018) to simulate intra-cranial EEG (iEEG) dynamics. Proximity to criticality is controlled by tuning relevant biophysically meaningful parameters. Near-criticality is required to reproduce the observed scale-free power spectrum of iEEG recordings (Chaudhuri et al., 2018). Setting the model closer to its critical point may account for the unique dynamics observed during free recall (Norman et al., 2017).

To provide further insight, Fig. 1 schematically illustrates critical slowing down (CSD) in a random recurrent neural network and in a one-dimensional non-linear system near its critical point. Figure 1A shows the expected activity in a random recurrent network at varying proximities to its critical point, as set by G. The critical point is defined by a network gain parameter $G = 1$. For a transient stimulus, activity will dissipate when the network gain is set to $G < 1$ (blue arrow), diverge to the maximal neuronal rate (in black dashed line) when $G > 1$ (green arrow), and tend to persist at enhanced slow fluctuation frequencies when $G \lesssim 1$, namely slightly below the critical point (yellow arrow). For a continuous signal, the steady-state power spectrum indicates an increase in the amplitude of slow activity only for $G \lesssim 1$.

Figures 1B & 1C further illustrate the CSD phenomenon in a one-dimensional system. The dynamics are characterized by a simple quadratic equation: $\mathrm{f}(x) = x^2 + r$, where x is a time-dependent variable satisfying $\frac{dx}{dt} = \mathrm{f}(x)$, and r is the system's control parameter. At $r = 0$ the system has a critical (bifurcation) point. For $r > 0$ it is super-critical, since at this domain there are no fixed points and x always diverges to infinity, whereas at $r < 0$ it is sub-critical and two fixed points arise at $x^* = \pm\sqrt{r}$ (Figure 1B; filled circles correspond to stable fixed points and hollow circles to unstable fixed points). Close to a given fixed point, the dynamics can be linearized and the deviation from the fixed point can be approximated by

$e^{t/\tau}$, where $\tau = 1/f'(x^*)$. The magnitude of the time constant that controls the dynamics approaches infinity as the system approaches its critical point (where $f'(x^*) = 0$). Thus, the dynamics slow down as the system approaches the critical point (Figure 1C).

In summary, we propose that the unique dynamics observed by Norman et al. (2017) may be accounted for by a closer proximity of the local cortical network to a critical point during free recall. This enhances the gain of the local network, making it more sensitive to external noise and driving it closer to the decision bound. We propose a model of a randomly connected recurrent network subject to intrinsic membrane potential noise for this putative mechanism. Our findings support the hypothesized slowing down modulation near-criticality. They support the hypothesis that the phenomenon of scale-free resting state fluctuations and their modulation during intrinsically motivated tasks reflect a basic and ubiquitous behavior common to all suitably configured recurrent systems.

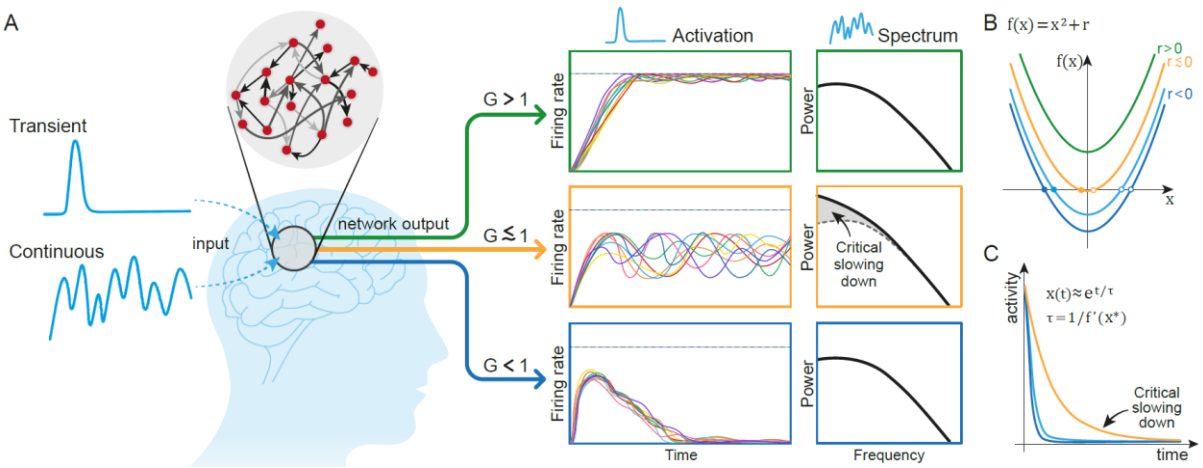

Figure 1. The impact of gain change on the dynamics of a recurrent system. The figure provides an illustrative and simplifying explanation of the critical slowing down (CSD) phenomenon in the dynamics of a recurrent system. CSD takes place as the system crosses between its sub-critical domain (G < 1, here depicted in blue) and its super-critical domain (G > 1, here in green). In this near-critical state (G ≲ 1, here depicted in yellow), when the system's gain (also termed 'control') parameter is increased to the vicinity of (but still below) the critical point, it displays cardinal slowing down and amplification of its dynamics. Panel 1A delineates the expected activity in a random recurrent network at varying proximity to its critical point. For a transient stimulus, activity in the network will (a) dissipate in the sub-critical domain (G < 1, in the bottom sub-panel) (b) diverge to the maximal neuronal rate (black dashed line) in the super-critical domain (G > 1, top sub-panel) and (c) tend to become

persistent as the gain approaches G $\lesssim$ 1 (middle sub-panel). For a continuous signal, the power spectrum will indicate rise in the amplitude of slow-wave activity only at the domain of G $\lesssim$ 1. Figures 1B & 1C provide further illustration of the CSD phenomenon exploring the dynamics of a simple one-dimensional non-linear system, driven by the quadratic equation of $f(x) = x^2 + r$. Panel 1B depicts the system and its solutions as the value of r, the control parameter is modified between super-critical (r > 0, in green), sub-critical (r < 0, blue) and near-critical (yellow, r $\lesssim$ 0) states. Panel C shows how the system dynamics slows down as r approaches 0. The curve corresponding to r > 0 diverges exponentially (not shown). See a more detailed discussion in the text.

Results

To model the iEEG signal, we simulated a sparse random recurrent network, realizing a firing rate model (see Methods). The summed activity of a sample of units represented the corresponding iEEG. The proximity to criticality was modulated through a control parameter, G, corresponding to the product of the network sparseness p, the neural gain, γ, and the mean synaptic strength μ_{conn}, with the critical transition from subcritical to supercritical domain expected at $G = \gamma p \mu_{conn} = 1$. We first examined whether our network model could reproduce the dynamical characteristics of the spontaneous resting state activity fluctuations as recorded in the human cortex, and found that it did when set close to its critical point (G = 0.94), as shown in Fig. 2. Figure 2a-b compare real iEEG recordings and simulated network dynamics. Panel 2a shows spontaneous firing rate fluctuations recorded from two auditory cortex neurons recorded across hemispheres during rest (obtained from Nir et al., 2008). Panel 2b shows examples of similarly correlated activity fluctuations of two simulated units in the recurrent network.

A more comprehensive qualitative comparison across the entire data set is shown in Fig. 2c-d. Here, instead of single neurons we use the broad band high frequency power fluctuations of the intra-cranially recorded local field potential (see Methods). It has been previously shown (Manning et al., 2009; Mukamel et al., 2005; Nir et al., 2007) that these fluctuations in power of the LFP in the high frequency broadband (HFB) provide a reliable index of the fluctuations in the average firing rates of neurons within the recording site. Note that this HFB measure should be distinguished from the direct recordings of the LFP signal itself.

The autocorrelation and cross-correlation PSD of the HFB obtained from auditory cortex across the two hemispheres during rest are shown in panel 2c, while panel 2d depicts the simulation of these activity fluctuations obtained in a network of 400 neurons. The probability for nonzero network connectivity was set to p = 0.2, and the mean synaptic strength to μ_{conn} = 49.881 (both parameters were kept fixed in all simulation results presented in this study). The time constant (τ) was set around 20 ms, which is close to well-known estimates for cortical neurons' membrane time constant (Gao et al., 2020; Koch et al., 1996; Softky & Koch, 1993). Results for the various values of τ explored to optimize the fit of the "knee" bend in the curve are presented in SI Fig. S2, showing τ values for 2, 20, and 200 ms. The gain parameter was set at γ = 0.094 Hz/pA, implying G = 0.9377 for best fit of the control parameter. The fraction of the network sampled (determining the exponent of the faster modes) was set at α = 0.05. For the power spectra of the auto- and cross-correlation computations, two distinct random samplings of αN neurons from the same simulation were obtained.

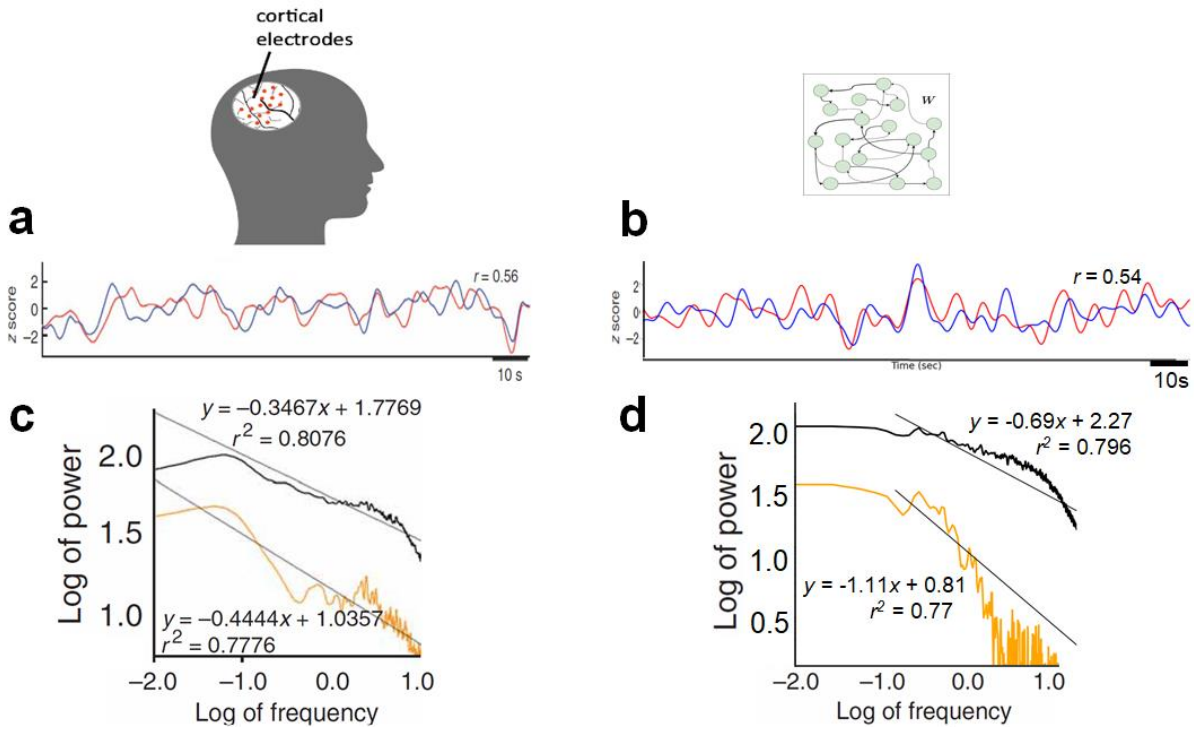

Figure 2. Ultra-slow spontaneous oscillations of neuronal activity in the brain and in a recurrent network simulation. Empirical iEEG results during wakeful-rest (adapted from Nir et al., 2008), presented here in panels a and c, are compared and contrasted with corresponding fitted simulation results in panels b and d, respectively, from an artificial neural

network model with 400 neurons. Panel a presents the HFB signal from homological left and right auditory cortices. Panel b demonstrates a corresponding signal from two highly correlated neurons in the artificial network. Panel c presents the autocorrelation (black line) of the HFB PSD and the cross-correlation (orange line) of this signal obtained across the two auditory cortex hemispheres. Panel d depicts, for comparison, our simulation of these activity fluctuations. Note the similar location of the knee frequency in the spectra of the empirical and simulated data (for further comparison see SI Fig. S2).

Following Nir et al., 2008, the autocorrelation was computed using signals from the first sampling only (resembling a single cluster of neurons in the network), and cross-correlation was computed iteratively between neuron pairs of both samples. Finally, the power spectrum was obtained by computing the mean of these autocorrelation (black line) and cross-correlation (orange line) curves (Methods). As can be seen, the simulated function was quite similar to the experimental brain recordings, although the curve's slope in the simulation was somewhat sharper than in the empirical results.

Next we examined whether the recurrent network simulation using the same value of τ (i.e. 20 ms) could also fit the baseline shift and amplitude amplification of the slow spontaneous fluctuations observed during targeted free behavior, as reported in (Norman et al., 2017). To that end, parameters of the simulated network were again fitted for optimal power spectrum match with results obtained by the intracranial HFB signal PSD.

Figure 3 compares the intra-cranially recorded HFB baseline shift amplification with the simulated neuronal activity using a network of 240 neurons (the parameters p and μ_{conn} were set to the same values as in the simulation presented in Fig. 2). As for the setting of the decay constant, in addition to the optimal knee-location fit obtained in Fig. 2 (with τ = 20 ms), another approximation method was employed, a Lorentzian approach, following (Chaudhuri et al., 2018). The result of this approximation is shown in SI Fig. S1. It was established once again, based on both methods, that setting this parameter near the biophysically-grounded-estimate of the membrane time constant optimizes the fit of the knee frequency location, and here also the PSD curve for mid-range frequencies (> 0.1 Hz and < 10 Hz). The sampling fraction was set to α = 0.01 to adjust the curve slope in the higher frequencies. The mean and std of I^{ext}, the noisy membrane potential related input, was ~20 (+/- 11.5) pA, and the simulation was run for 1800 s, with the first 600 s omitted as a stabilization period before analysis of the remaining 1200 s.

Panel 3a depicts an example of the experimentally derived spontaneous HFB fluctuations in two neuronal populations - one that was targeted to elicit free recall (red) and the other that was not targeted (green). The baseline shift of the fluctuations for the targeted area is readily visible. For comparison, Panel 3b shows the simulated activity fluctuations for a network when a uniform baseline (fixed value) shift, I^{add} (see Methods), was added to the white noise inputs (red) and without this added fixed value shift (green). Note the gap between the two curves can easily be fine-tuned via setting the relative value and ratio of I^{ext} and I^{add}, without compromising other measurable properties.

Panel 3c provides a more comprehensive analysis by showing the PSD, obtained from all intra-cranially recorded sites in the targeted neuronal population (red PSD) vs. the non-targeted population (blue PSD). To make the comparison of these neuronal recordings to the simulations easier, we overlay the simulated results on top of the brain recordings in panel 3d, in which the mean and standard deviation for multiple realizations (specifically, 8 arbitrary random-seed network connectivity initializations) of simulated target (yellow) vs non-target (green) blocks is presented. Here, the fit in PSD was reached by adding a fixed value shift I^{add} of 12.5 pA to the white noise during simulated targeted (orange thick curve) but not to the non-targeted blocks (green thick curve). As in (Norman et al., 2017), the increase in the power of the ultra-slow modulation in the simulated PSD amplitude during recall relative to rest blocks over the different realization was statistically significant (for the range < 0.2 Hz; p < 0.05, FDR corrected, signed-rank test).

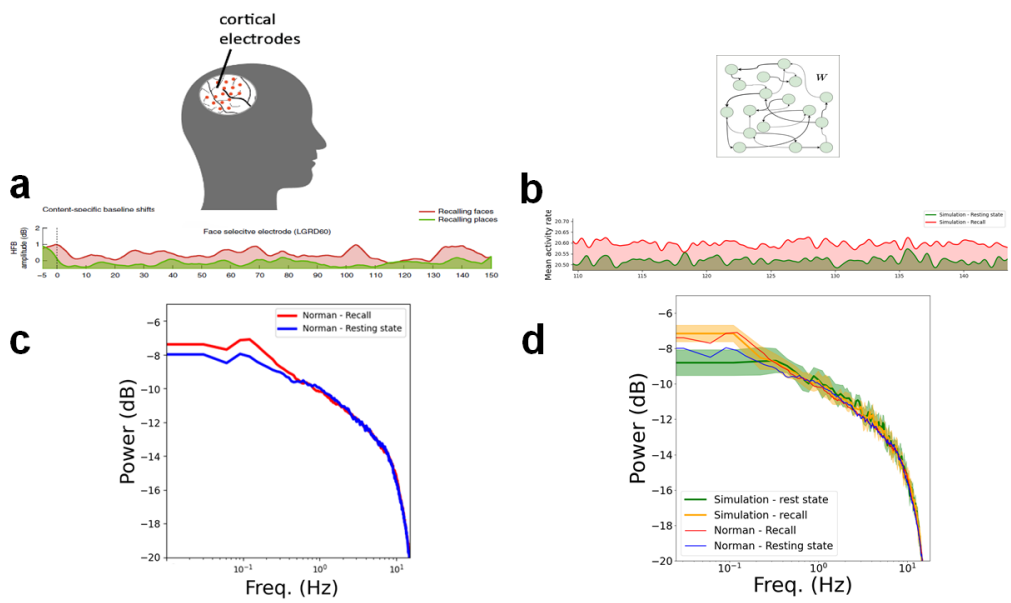

Figure 3. Amplification of slow-fluctuations in the brain and in the recurrent network. iEEG HFB signal from targeted free recall target (red) and non-targeted (green) neuron populations (adapted from Norman et al., 2017) in panel a, is compared with the simulated spontaneous activity in "recall" target (with additive noise) vs non-target "rest" blocks in panel b. The power spectra obtained from all intra-cranially recorded free-recall target sites (red) relative to the non-targeted population (blue) is shown in panel c. Simulated results are overlaid on the empirical PSD results in panel d, showing near fit, in expectation, over multiple realizations. The mean and standard deviation are shown for the free-recall target (yellow) and non-target (green).

Interestingly, an alternative simulation approach to slowing down the near-critical dynamics led to similar amplification in the targeted ultra-slow frequency PSD. Here, a more direct modulation was implemented, increasing the connectional efficacy by a small uniform factor. In fact, it was enough to increase the network gain by ~1%, from 0.94 to 0.95, to reproduce the empirically observed enhancement of slow frequencies during free recall. In SI Fig. S3 we show distinct single realization PSD results from these simulations using the same color scheme mentioned above. Note the similarity in modulations of the PSD, and, specifically, the amplification in the ultra-slow-frequency domain of the PSD, evident in the targeted relative to non-targeted simulated blocks.

To examine the impact of network connectivity on the PSD in detail we have systematically examined the influence of changing connectivity parameters. This is depicted in Fig. 4. In panels 4a-b, a simplified network setting with 100 neurons was used to explore the influence of the connectivity control parameter G, via gradual adjustments of γ, on the spectra while keeping all other parameters fixed. The simulation lasted 800 s, with the first 200 s omitted in analysis to allow signal stabilization; τ was set to 20 ms, and α was set to 1.0.

Panel 4a shows the effect of setting G over its full range from 0.0 to 1.0, whereas panel 4b focuses on the narrow range near the critical point. Two key findings emerge from this analysis: first, a gradual increase in the amplitude of slow frequencies that accelerates near the critical point of G (when $G \lesssim 1$); and second, the linear, medium to high frequency range of the PSD remains unchanged even when all network connections are set to zero, effectively isolating the neurons from each other. In panel 4c, the PSD results for the same simulation as in Fig. 3 are shown, but with gradually increasing levels of baseline shift to the

noisy input, I^{ext}. Similar to the modulation of connectivity strength towards criticality in G, the additive noise leads to a slowdown in ultra-slow frequencies only.

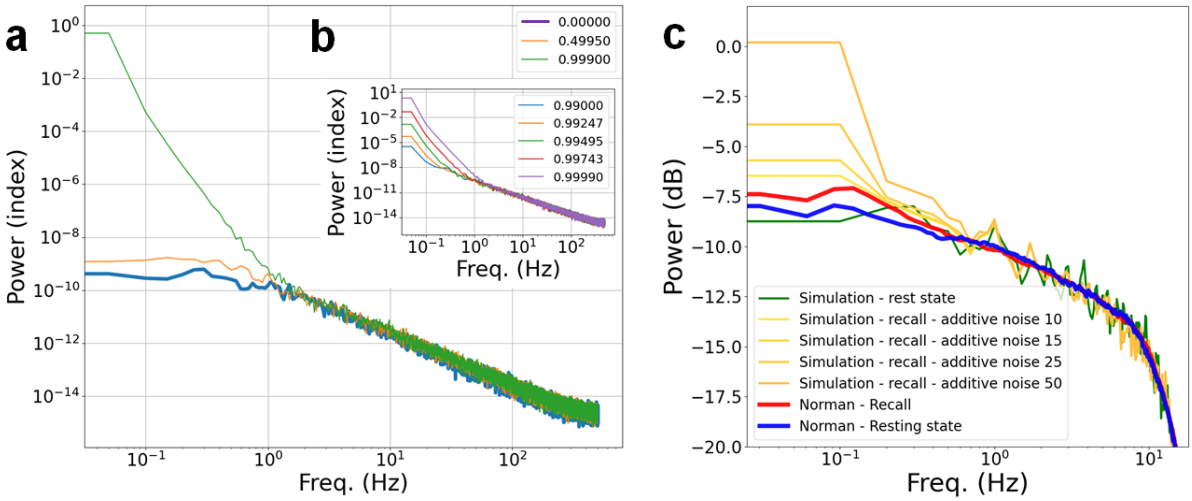

Figure 4. Effect of network connectivity strength and additive noise on spontaneous fluctuations' PSD. Panels a and b demonstrate the critical slowing down of low-range frequencies in an arbitrary network setting as the control parameter approaches the value of 1. In panel a, the case of 0-connectivity (i.e. $\gamma = 0$) is included (blue bold) and in the inset (panel b), the gradual near-criticality slowing down is highlighted. Panel c shows a similar critical slowing down effect, here as a function of the amount of additive noise (see Methods I^{add}) overlaid on PSD results from (Norman et al., 2017).

The emergence of a scale-free power-law in the fluctuations of simulated activity (even in individual isolated neurons) raises the concern that the network behavior merely reflected the dynamical structure of the injected input noise. To examine this possibility, we modified the injected noise profile by high-pass filtering and observed the effect on the network PSD for parameters near criticality. The simulation was 800 s long, with the first 200 s excluded for signal stabilization. The time constant τ was set to 20 ms, and α to 1.0. Figure 5 displays the simulation results. We also used the same noise profiles to simulate isolated neurons (zero-connectivity network), with the resulting PSD shown in SI Fig. S4.

As can be seen, even drastic changes in the spectral power profile of the input noise had only minor impact on the PSD mid-to high frequency power-law profile of the network as a whole. This is evident in the striking discrepancy between the PSD profile of the input noise (Figure 5 insets c-d) and the PSD of the entire network (panels 5a-b). Of particular interest is

the insensitivity of the network even when all slow input frequencies were drastically quenched to a tenth of its original power (see panel 5a relative to 5c). Similar behavior for the PSD of mid-to-high range frequencies is preserved also in the isolated neuron network (SI Fig. S4).

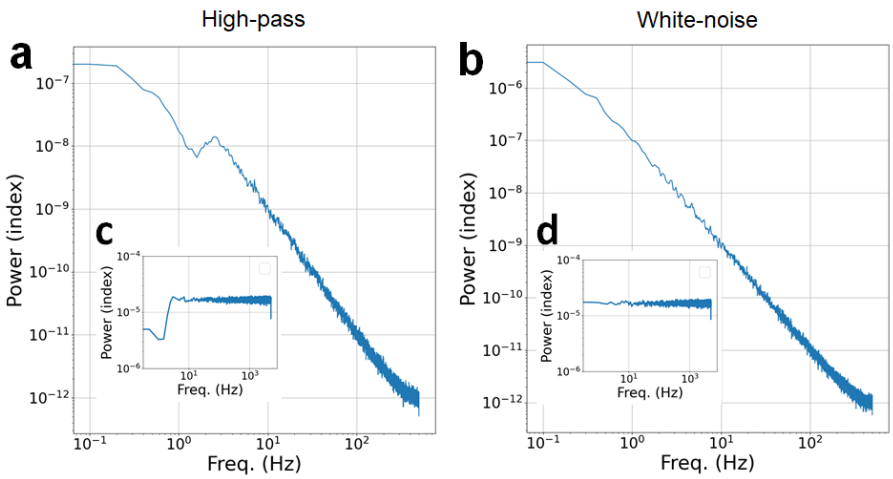

Figure 5. Impact of changes in input noise spectral profile on the network PSD. Panels a-b demonstrate the simulated network PSD when the injected noise is high-pass filtered (panel a) relative to the initial unfiltered white noise (panel b). Insets c – d present the noise spectra in use for each of the main panels, respectively.

To analyze the influence of network parameters on the amplification of the spontaneous fluctuations' slow frequencies - i.e. the slowing down near criticality, we scanned the parameter space of network connectivity and size. In the analysis, we iteratively generated network realizations of larger and larger scale, and increased the control parameter G (via γ) from subcritical to near-critical range, while collecting the slow (normalized by fast) frequency power values.

The results are shown as a two-dimensional heat map (Fig. 6). The x and y axes in this map depict network size and control parameter settings, respectively, whereas the color per pixel denotes the degree of slow frequency amplification (more details in Methods). As can be seen, both parameters had a powerful amplification effect on the slow-frequency power. Amplification became more pronounced only when approaching criticality (i.e., $G > 0.95$), but interestingly, this was limited to networks larger than 10 neurons. Small networks often showed a mild reduction in slow frequencies near the dynamical transition point.

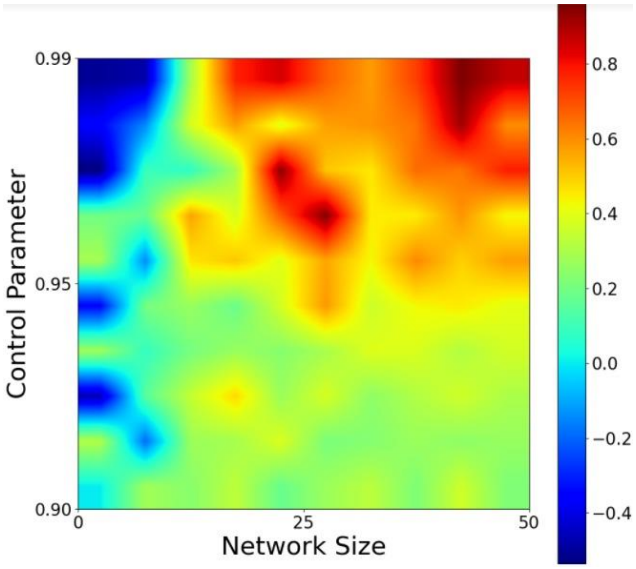

Figure 6. The impact of network size and network connectivity strength on the amplification of the slow spontaneous activity fluctuations. The map color scheme presents this amplification as slow frequency power, normalized by fast frequency power. Each of the cells represents an average of five random realizations, per specific network size and control parameter value.

Discussion

Ultra-slow spontaneous fluctuations are one of the most widely studied phenomena of the human brain. Numerous studies have revealed that these fluctuations are organized along highly complex but informative connectivity patterns (Fox et al., 2006; Fox & Raichle, 2007; Sadaghiani & Kleinschmidt, 2013; Strappini et al., 2019) suggested to be related to cognitive habits, traits and pathologies (Eldar et al., 2013; Hahamy et al., 2021; Harmelech & Malach, 2013). It is also proposed that they drive self-generated, voluntary, and creative behaviors (Broday-Dvir & Malach, 2021; Norman et al., 2017; Norman & Malach, 2022).

Despite extensive research on the properties and dynamics of these slow fluctuations (Fox & Raichle, 2007; Nir et al., 2008; Raichle, 2011; Raut et al., 2021), the underlying neuronal mechanism remains unknown. The slow dynamics and intricate organization of these fluctuations may suggest a complex underlying mechanism, but we argue that the opposite is true. We propose that intrinsic fluctuations in recurrent networks exhibit a basic physical principle that leads to their slowing down and amplification of amplitude as the network approaches its critical point, a phenomenon known as critical slowing down. We hypothesize

that this fundamental dynamics underlie the behaviors of the ultra-slow spontaneous fluctuations.

Using a simple random recurrent network near criticality and unstructured white noise inputs, we successfully simulated the critical slowing down dynamics and reproduced the power spectrum of the spontaneous activity fluctuations as reflected in the intracranially measured HFB. Furthermore, a small uniform increase in synaptic efficacy, or alternatively, a small DC shift in this noise input, near the critical transition point of the network dynamics, were sufficient to simulate the amplitude enhancement documented during targeted free recall in the visual cortex.

Based on the success of our simulations, we propose that the original driver of slow spontaneous fluctuations in neuronal activity is stochastic noise originating in each individual neuron, which then accumulates through the recurrent connectivity structure. The exact source of this noise is unknown and may derive from numerous processes, such as thermal, synaptic, and channel fluctuations (Rusakov et al., 2020; Yarom & Hounsgaard, 2011). All these processes could contribute to the random membrane potential fluctuations consistently observed across all types of cortical neurons (Lampl et al., 1999; Raichle, 2011; Yarom & Hounsgaard, 2011).

In this work, we simulated two key features of spontaneous fluctuations: their power spectra and modulation during an intrinsically motivated task. However, we did not address how complex functional connectivity patterns emerge from such noise fluctuations. We have previously suggested that these patterns are shaped by synaptic structures and reflect prior learning (Harmelech et al., 2013; Harmelech & Malach, 2013). This hypothesis predicts that a recurrent network with updatable connectivity based on suitable learning rules will spontaneously reproduce a repeatedly activated specific pattern when network neurons, having learned the pattern, are injected with white noise near criticality. While we focus on the power spectra and modulation during task-induced targeting of categorical boundaries, future simulations could investigate the emergence of such functional connectivity patterns.

Earlier studies have demonstrated the emergence of a scale-free 1/f power-law spectrum using a rate model simulation near criticality (Chaudhuri et al., 2018; Gao et al., 2020). However, they focused primarily on the tipping point of criticality ($G \approx 1$) of the network parameter setting. In contrast, we aimed to investigate the minimal conditions required for

the scale-free PSD to arise, examining network connectivity weights far below the critical point, as well as the impact of the intrinsic membrane noise profile on the network's neuronal activity.

Intracranial recordings of single neurons and the high frequency broadband (HFB) amplitudes of the LFP, which has been shown to index the average firing rate of cortical neurons (Manning et al., 2009; Nir et al., 2007), reveal the power spectra of the spontaneous fluctuations in the human cerebral cortex during rest (Figure 2c and 3c). These spectra consist of two power-law exponents, with slower frequencies following a shallower exponent than higher frequencies. Remarkably, a similar profile emerges in a random recurrent network with fully stochastic connection strengths and input noise under the appropriate parameters (compare to Fig. 2d and 3d).

These results were obtained using minimal biophysically-oriented parameter settings, consisting of a physiologically plausible membrane time constant (~20 ms), sampling of only a small part of the network nodes (α), which is compatible with the localized nature of the empirical recording sites, and control of the system's slowing down by a single gain parameter (G).

We first discuss the high frequency slope of the HFB PSD. Analyzing the behavior of the network under zero connectivity (Fig. 4A) revealed that the resultant fluctuations in membrane potential approximated a power-law beyond a certain “knee” frequency, even when the spectra of the stochastic noise injected into each neuron was flat (white noise) or biased towards higher frequencies (see Methods and SI Fig. S4). Thus, the neuron, even when decoupled from the rest of the network, maintains the slow frequency band and attenuates the higher frequencies in a scale-free manner. A mathematical analysis presented in SI section 1 shows that the dynamics of a scale-free power spectrum with an exponent of -2 is indeed the expected result for the fast-mode HFB PSD. Recent studies of activity fluctuations in isolated cortical and hippocampal neurons also reveal that individual neurons are capable of generating stochastic fluctuations obeying scale-free power-law profiles as well as long time-scales, even in the absence of network connections (Gal et al., 2010; Gal & Marom, 2013a; Sukenik et al., 2021).

Examining the impact of network connectivity on the spontaneous fluctuations reveals a specific amplification of slow frequencies' amplitude in the spontaneous fluctuations spectra

as the network approaches its dynamical phase transition point. This is shown when separately examining the impact of changing the connectivity strength, i.e., the efficacy of intra-neuronal communication weight, and the richness of connectivity as reflected in network size (Fig. 6). A successful amplification of slow frequencies can only be achieved within a regime in which these two parameter spaces overlap. However, only random network configurations were explored in this study, and a better structured connectome arrangement, whether shaped by innate prearrangement or as learned by prior experiences, may present other near-critical behaviors. Nevertheless, it should be noted that even in extremely small, properly configured networks possessing fewer than 20 neurons, a powerful amplification of ultra-slow fluctuations can be obtained, suggesting that ultra-slow fluctuations lasting many seconds do not necessarily depend on large-scale cortical networks for their generation, as also suggested by previous work (Gal & Marom, 2013b).

As discussed in the introduction, the spontaneous fluctuations are selectively amplified when behavior is intentionally confined to a specific category. For example, when participants attempt to visualize different items belonging to a certain category of visual stimuli, their slow spontaneous fluctuations get amplified specifically in the targeted representation during the recall period (See Figure 3a and 3c and more details in Norman et al., 2017). Such amplification enhances the probability of these fluctuations to cross the decision bound in the category-selective area, providing an elegant mechanism for rapid and flexible control over the expression of any spontaneous behavior within an intentionally selected categorical boundary. Thus, when we try to freely come up with images of different apples, we rarely imagine, by mistake, an orange. As we show here, critical slowing down provides a ready mechanism for such behaviors.

When local populations' activity fluctuations transiently cross the decision bound, this may lead to rapid self-amplification termed "local ignition". Such ignitions have been experimentally observed during crossing the perceptual awareness threshold using iEEG recordings (Fisch et al., 2009; Moutard et al., 2015). Additionally, near a critical point, network sensitivity increases, enabling better encoding and recall of information through balanced response to inputs and adaptation to noise (Kim et al., 2021; Shriki & Yellin, 2016).

Our simulations of a random recurrent network demonstrate that a simple shift in gain modulation or noise level accurately reproduces the intra-cranially recorded slow frequency

amplification during category-selective visual recall (Fig. 3d and SI Fig. S3). The key factor inducing the amplification effect is the network's proximity to its critical transition point, regardless of the specific mechanism controlling its excitation.

It is important to note that empirical brain data and recurrent network simulations specifically relate to fluctuations in neuronal firing rate or, in cases where such measures are unavailable, to the broadband high frequencies (gamma) envelope of the LFP. Previous studies have shown that the gamma envelope reflects fluctuations in the average firing rates of local neuronal populations (Manning et al., 2009; Nir et al., 2007). These measures of firing rate fluctuations should be distinguished from fluctuations in the local field potential, i.e., the LFP, itself. Thus, it should be emphasized that the power-spectrum of the LFP should not be confused with the power spectrum of the firing rate or HFB fluctuations, as the two types of fluctuations can be antagonistic to each other under different experimental paradigms (Privman et al., 2011).

Moreover, previous studies have suggested that the LFP power spectrum is optimally fitted by setting the dynamics control parameter precisely at the tipping point of criticality (i.e. at $G = 1$), which could potentially imply fundamental instability and a network easily crossing between subcritical to supercritical states (Chaudhuri et al., 2018; Gao et al., 2020). However, our optimal fit for the HFB power spectra implies that relevant cortical networks operate below this critical transition point (i.e., at $G{\sim}0.94$), where stability is still maintained but close enough to critical dynamics to allow the system to computationally benefit from near-criticality effects.

Finally, it is worth noting that the relationship between the LFP and firing rates is more appropriately captured by measuring the changes in the exponent of the LFP power-law PSD, as observed in our previous intra-cranial analysis of visual responses (Podvalny et al., 2015). While these issues could potentially be examined in our recurrent network simulations, they have not been pursued in this work.

Overall, the findings from our simulations suggest that the ultra-slow spontaneous fluctuations are an emergent network phenomenon and support the idea that the cortex operates near a critical point, allowing for rapid and flexible control over spontaneous behaviors while maintaining stability. Furthermore, they provide a ready mechanistic explanation for the observation that targeting of specific categories of behavior amplifies the

slow band of the spontaneous activity fluctuations. This work opens new avenues for investigating the role of criticality in brain function and could potentially lead to the development of new computational models for understanding the neural basis of cognition and behavior.

Methods

Random recurrent network as a rate model

Rate models can be derived from the well-studied Wilson-Cowan equations (Wilson & Cowan, 1972). They were explored within the context of iEEG data in recent literature (Chaudhuri et al., 2018; Gao et al., 2020). In previous work (Shriki et al., 2003), we have shown that such rate models can be faithfully derived from large-scale conductance based networks resembling cortical organization. In this type of rate models, the dynamic variable that characterizes the neuronal activity is the firing rate of the neuron, i.e., the number of electrical pulses (action potentials) in a unit of time. The simplicity of rate models makes them highly useful in studying properties of large networks.

Here, we considered a random recurrent network model consisting of N rate-based units representing single neurons or groups of neurons (see Figures 2-6). We closely follow the model proposed in (Chaudhuri et al., 2018) to explain the power spectrum of iEEG recordings. The firing rate dynamics of the *j*-th neuron's output over time in this model is given by:

$$\tau \frac{d}{dt} r_j(\mathrm{t}) = -r_j(t) + \gamma \left[\sum_{j=1}^{N} W_{jk} r_j + I_j^{ext}(t) \right]_+ \qquad j = 1 \dots N \qquad (1)$$

where r_j is the firing rate of the *j*-th unit activity level, and τ is a characteristic integration time. The $[\ ]_+$ brackets denote a rectified linear (ReLU) activation function. The γ variable denotes the slope of the firing rate – current curve (f-I curve). The weights W_{jk} describe the strength of the connection from the presynaptic unit k to the postsynaptic unit *j*, and I_j^{ext} denotes the external input to the *j-th* unit (drawn here randomly from a "standard normal" distribution).

Criticality in the random recurrent network

We consider a network architecture comprising a non-hierarchical cluster of recurrently connected neurons characterized by a semi-linear f-I curve with gain γ. Following (Chaudhuri et al., 2018), we choose the connections in this network (the entries of matrix *W*) to be sparse and random. More specifically, each entry is nonzero with probability *p*, and the nonzero entries are drawn from a normal distribution, with positive mean μ_{conn} and variance σ_{conn}, normalized by the size of the network, N.

When set as a rate model (assumed to be represented by the iEEG high-frequency broadband power modulation), we hypothesize it depicts the summed recurrent synaptic current into a fraction of neurons in this network, along with an intrinsic complementary membrane noise. Previous work (Chaudhuri et al., 2018) demonstrated how the product of three main parameters control the proximity to the network's critical branching point. These are: μ_{conn}, γ, and *p.* At the tipping point of criticality, they satisfy the relation $\gamma p \mu_{conn} = 1$, see (Chaudhuri et al., 2018). Thus, we define a control parameter $G = \gamma p \mu_{conn}$, and require that it lies in the vicinity of the critical point - $G \lesssim 1$. In a near-critical state, either one of these arguments composing the control parameter could be varied to yield similar results towards the crossing point into a supercritical state.

To provide additional insight in the present context, we note that near a steady-state, an algebraic linearized approximation of the spontaneous fluctuations dynamics can be obtained. We briefly summarize the details given in (Chaudhuri et al., 2018):

1. The eigenvalue spectrum of such random matrices is composed of a cluster of complex eigenvalues with negative real part, and a single isolated eigenvalue, which corresponds to the uniform eigenvector (namely, to the mean network activity).
2. This approximation is characterized by a matrix whose dominant eigenvalue converges ever closer to 0 as the system approaches its bifurcation point.

Critical slowing down is manifested in the system's temporal dynamics, as they are linked to the inverse of the abovementioned dominant eigenvalue (see SI for additional detail). As the system approaches criticality, signals reverberate in the network for increasingly longer time,

producing a slowly decaying autocorrelation function and increasing the power of low frequencies.

For sake of convenience, the following parameters were kept fixed across all simulation runs presented in the paper: μ_{conn} = 49.881 pA/Hz, σ_{conn} = 4.988 pA/Hz, p = 0.2. Unless otherwise noted, the parameter that was used to control the proximity to criticality was the slope of the f-I curve, γ. We did however verify that qualitatively equivalent results can be reached by modifying G using other parameters.

The characteristic integration time and PSD profile's pattern

As for the characteristic integration time τ, we explored values in the range of 2 – 200 ms. Using a simple linearized mathematical approximation (see SI Fig. S1 and (Chaudhuri et al., 2018)) it can be shown that the commonly observed "knee"-bend in in the power spectral density (PSD) profile appears near $f_{knee} = \frac{1}{2\pi\tau}$, and that modulation of slow-frequencies is also significantly influenced by this the integration time constant, implying that the fit tuning process should carefully consider its setting.

Our findings here indicate that using the previously reported timescale of the membrane time constant in the proximity of τ = 20 ms (Gao et al., 2020; Koch et al., 1996; Softky & Koch, 1993) led to an optimal fit regarding the location of this knee in the activity rate PSD curve as well as the related slow frequencies slope. That is, for both of the cases explored in (Nir et al., 2008; Norman et al., 2017), as demonstrated in Figure 2 and 3 respectively.

The parameter α, defined as the fraction (i.e. 0 < α < 1) of network nodes selected for summation, plays a significant role in determining the slope of medium range frequencies (> 0.1 Hz and < 10 Hz) in the PSD curve, since it influences the mixture of slow and fast dynamical modes exposed in the system. When constructing the PSD, we sum the activities of α*N* random nodes and compute the spectrum of the summed activity. The larger the value of α, the larger the contribution of the dominant slow mode to the mid-range PSD slope, since this mode is shared among the network nodes.

Simulation and parameter fitting efforts

Simulation code, including full implementation of the rate model and plotting of figures, was developed in Python, taking advantage of suitable open-sourced libraries' methods (including, but not limited to, SciPy and Matplotlib), facilitating tuning efforts for fitting the empirical results (details below).

For the results depicted in Fig. 2, the signal was low-pass filtered (for < 0.1 Hz) as in (Nir et al., 2008), using a Butterworth method. Correlation, auto- and cross-correlation coefficients were computed using time-lagged correlation methods. In panel 2b, the activity of two arbitrarily selected highly-correlated neurons is presented. In panel 2d, the power spectrum was computed using Matplotlib mlab's PSD, implementing the Welch method. A simple amplitude scaling factor k was applied to match the Welch method results with those presented by direct use of FFT power in (Nir et al., 2008). A regression line curve was fitted using a curve-fitting method in the range of 0.1 – 10 Hz.

For Fig. 3, the simulation was arranged as consecutive "rest" vs "free-recall" 1800 s blocks. Additive noise I^{add} was defined as constant value within each simulation run, so that $I_{new}^{etx} = I^{ext} + I^{add}$. For the purpose of sampling a satisfactory distribution for statistical analysis, the simulation was repeated using different random seed values. The multiple realizations generated were independently compared with the empirical data. Other than that, similar simulation and computational methods were applied as in Fig. 2. Testing for various possible confounds, the simulation configuration for the results presented in Figures 4 – 6 was suitably adapted, but remained similar in concept to the settings in Fig. 3. In data preparation for Fig. 5, white noise was sampled in advance, applying suitable filters (using scipy signal.butter methods) over the random (white noise) normal distribution based temporal signal. For the map presented in Fig. 6, we iterated through the parameter space of network connectivity and size, iteratively generating random network realizations of larger and larger scale. Thus, as the control parameter G was modified (via γ) from subcritical to near-critical range, values of the slow (normalized by fast) frequency power modulation were collected.

The human iEEG data and its analysis

The empirical data used in this study has been previously reported in (Nir et al., 2008 and Norman et al., 2017). In both studies, intracranial recordings were obtained from patients with pharmacologically resistant epilepsy who were undergoing a surgical evaluation process for the treatment of their condition. In the first study (Nir et al., 2008), data were recorded from five participants (over multiple sessions) under the conditions of wakeful rest. During the wakeful rest, subjects' eyes were closed and the room was dark and quiet, however, alertness was occasionally monitored. The second study (Norman et al., 2017) included twelve participants who performed a free recall task, as follows. Immediately after a 200 s period of closed-eyes resting state, participants were presented with 14 different pictures of famous faces and popular landmarks in a pseudorandom order (each picture was repeated four times, and shown for 1500 ms, with 750 ms inter-stimulus interval). After viewing the pictures, participants put on a blindfold (or closed their eyes) and began a short interference task of counting back from 150 in steps of 5 for 40 s. Upon completion, recall instructions were presented, guiding the patients to recall items from only one category at a time, starting with faces in one run and with places in a second run. Participants were asked to verbally describe each picture they recall, as soon as it comes to mind, with 2–3 prominent visual features. The duration of this free recall phase was 2.5 min per each category. In both experiments analyses of iEEG data were focused on changes in high-frequency broadband amplitude (HFB, also known as high-gamma, defined as the range 40-100 Hz in the first study and 60-160 Hz in the latter one), shown to be a reliable marker of local neuronal population activity (Nir et al., 2007).

References

Arviv, O., Goldstein, A., & Shriki, O. (2015). Near-Critical Dynamics in Stimulus-Evoked Activity of the Human Brain and Its Relation to Spontaneous Resting-State Activity. *Journal of Neuroscience*, *35*(41), 13927–13942. https://doi.org/10.1523/JNEUROSCI.0477-15.2015

Arviv, O., Medvedovsky, M., Sheintuch, L., Goldstein, A., & Shriki, O. (2016). Deviations from Critical Dynamics in Interictal Epileptiform Activity. *Journal of Neuroscience*, *36*(48), 12276–12292. https://doi.org/10.1523/JNEUROSCI.0809-16.2016

Beggs, J. M. (2022). *The cortex and the critical point: Understanding the power of emergence*. The MIT Press.

Beggs, J. M., & Plenz, D. (2003). Neuronal Avalanches in Neocortical Circuits. *The Journal of Neuroscience*, *23*(35), 11167–11177. https://doi.org/10.1523/JNEUROSCI.23-35-11167.2003

Bertschinger, N., & Natschläger, T. (2004). Real-Time Computation at the Edge of Chaos in Recurrent Neural Networks. *Neural Computation*, *16*(7), 1413–1436. https://doi.org/10.1162/089976604323057443

Broday-Dvir, R., & Malach, R. (2021). Resting-State Fluctuations Underlie Free and Creative Verbal Behaviors in the Human Brain. *Cerebral Cortex*, *31*(1), 213–232. https://doi.org/10.1093/cercor/bhaa221

Buzsáki, G. (2006). *Rhythms of the Brain*. Oxford University Press. https://doi.org/10.1093/acprof:oso/9780195301069.001.0001

Chaudhuri, R., He, B. J., & Wang, X.-J. (2018). Random Recurrent Networks Near Criticality Capture the Broadband Power Distribution of Human ECoG Dynamics. *Cerebral Cortex*, *28*(10), 3610–3622. https://doi.org/10.1093/cercor/bhx233

Deco, G., & Jirsa, V. K. (2012). Ongoing Cortical Activity at Rest: Criticality, Multistability, and Ghost Attractors. *The Journal of Neuroscience*, *32*(10), 3366–3375. https://doi.org/10.1523/JNEUROSCI.2523-11.2012

Dotan, A., & Shriki, O. (2021). Tinnitus-like “hallucinations” elicited by sensory deprivation in an entropy maximization recurrent neural network. *PLOS Computational Biology*, *17*(12), e1008664. https://doi.org/10.1371/journal.pcbi.1008664

Eldar, E., Cohen, J. D., & Niv, Y. (2013). The effects of neural gain on attention and learning. *Nature Neuroscience*, *16*(8), 1146–1153. https://doi.org/10.1038/nn.3428

Fekete, T., Hinrichs, H., Sitt, J. D., Heinze, H.-J., & Shriki, O. (2021). Multiscale criticality measures as general-purpose gauges of proper brain function. *Scientific Reports*, *11*(1), 14441. https://doi.org/10.1038/s41598-021-93880-8

Fekete, T., Omer, D. B., O’Hashi, K., Grinvald, A., van Leeuwen, C., & Shriki, O. (2018). Critical dynamics, anesthesia and information integration: Lessons from multi-scale criticality analysis of voltage imaging data. *NeuroImage*, *183*, 919–933. https://doi.org/10.1016/j.neuroimage.2018.08.026

Fisch, L., Privman, E., Ramot, M., Harel, M., Nir, Y., Kipervasser, S., Andelman, F., Neufeld, M. Y., Kramer, U., Fried, I., & Malach, R. (2009). Neural “Ignition”: Enhanced Activation Linked to Perceptual Awareness in Human Ventral Stream Visual Cortex. *Neuron*, *64*(4), 562–574. https://doi.org/10.1016/j.neuron.2009.11.001

Fox, M. D., Corbetta, M., Snyder, A. Z., Vincent, J. L., & Raichle, M. E. (2006). Spontaneous neuronal activity distinguishes human dorsal and ventral attention systems. *Proceedings of the National Academy of Sciences*, *103*(26), 10046–10051. https://doi.org/10.1073/pnas.0604187103

Fox, M. D., & Raichle, M. E. (2007). Spontaneous fluctuations in brain activity observed with functional magnetic resonance imaging. *Nature Reviews Neuroscience*, *8*(9), 700–711. https://doi.org/10.1038/nrn2201

Gal, A., Eytan, D., Wallach, A., Sandler, M., Schiller, J., & Marom, S. (2010). Dynamics of Excitability over Extended Timescales in Cultured Cortical Neurons. *Journal of Neuroscience*, *30*(48), 16332–16342. https://doi.org/10.1523/JNEUROSCI.4859-10.2010

Gal, A., & Marom, S. (2013a). Entrainment of the Intrinsic Dynamics of Single Isolated Neurons by Natural-Like Input. *Journal of Neuroscience*, *33*(18), 7912–7918. https://doi.org/10.1523/JNEUROSCI.3763-12.2013

Gal, A., & Marom, S. (2013b). Self-organized criticality in single-neuron excitability. *Physical Review E*, *88*(6), 062717. https://doi.org/10.1103/PhysRevE.88.062717

Gao, R., van den Brink, R. L., Pfeffer, T., & Voytek, B. (2020). Neuronal timescales are functionally dynamic and shaped by cortical microarchitecture. *ELife*, *9*, e61277. https://doi.org/10.7554/eLife.61277

Gilaie-Dotan, S., Hahamy-Dubossarsky, A., Nir, Y., Berkovich-Ohana, A., Bentin, S., & Malach, R. (2013). Resting state functional connectivity reflects abnormal task-activated patterns in a developmental object agnosic. *NeuroImage*, *70*, 189–198. https://doi.org/10.1016/j.neuroimage.2012.12.049

Hahamy, A., Behrmann, M., & Malach, R. (2015). The idiosyncratic brain: Distortion of spontaneous connectivity patterns in autism spectrum disorder. *Nature Neuroscience*, *18*(2), 302–309. https://doi.org/10.1038/nn.3919

Hahamy, A., Wilf, M., Rosin, B., Behrmann, M., & Malach, R. (2021). How do the blind 'see'? The role of spontaneous brain activity in self-generated perception. *Brain*, *144*(1), 340–353. https://doi.org/10.1093/brain/awaa384

Haimovici, A., Tagliazucchi, E., Balenzuela, P., & Chialvo, D. R. (2013). Brain Organization into Resting State Networks Emerges at Criticality on a Model of the Human Connectome. *Physical Review Letters*, *110*(17), 178101. https://doi.org/10.1103/PhysRevLett.110.178101

Harmelech, T., & Malach, R. (2013). Neurocognitive biases and the patterns of spontaneous correlations in the human cortex. *Trends in Cognitive Sciences*, *17*(12), 606–615. https://doi.org/10.1016/j.tics.2013.09.014

Harmelech, T., Preminger, S., Wertman, E., & Malach, R. (2013). The Day-After Effect: Long Term, Hebbian-Like Restructuring of Resting-State fMRI Patterns Induced by a Single Epoch of

Cortical Activation. *Journal of Neuroscience*, *33*(22), 9488–9497. https://doi.org/10.1523/JNEUROSCI.5911-12.2013

Harris, T. E. (2012). *The theory of branching processes*. Springer-Verlag.

He, B. J. (2014). Scale-free brain activity: Past, present, and future. *Trends in Cognitive Sciences*, *18*(9), 480–487. https://doi.org/10.1016/j.tics.2014.04.003

Kim, M., Kim, H., Huang, Z., Mashour, G. A., Jordan, D., Ilg, R., & Lee, U. (2021). Criticality Creates a Functional Platform for Network Transitions Between Internal and External Processing Modes in the Human Brain. *Frontiers in Systems Neuroscience*, *15*, 657809. https://doi.org/10.3389/fnsys.2021.657809

Kinouchi, O., & Copelli, M. (2006). Optimal dynamical range of excitable networks at criticality. *Nature Physics*, *2*(5), 348–351. https://doi.org/10.1038/nphys289

Koch, C., Rapp, M., & Segev, I. (1996). A Brief History of Time (Constants). *Cerebral Cortex*, *6*(2), 93–101. https://doi.org/10.1093/cercor/6.2.93

Lampl, I., Reichova, I., & Ferster, D. (1999). Synchronous Membrane Potential Fluctuations in Neurons of the Cat Visual Cortex. *Neuron*, *22*(2), 361–374. https://doi.org/10.1016/S0896-6273(00)81096-X

Lee, K.-E., Lopes, M. A., Mendes, J. F. F., & Goltsev, A. V. (2014). Critical phenomena and noise-induced phase transitions in neuronal networks. *Physical Review E*, *89*(1), 012701. https://doi.org/10.1103/PhysRevE.89.012701

Legenstein, R., & Maass, W. (2007). Edge of chaos and prediction of computational performance for neural circuit models. *Neural Networks*, *20*(3), 323–334. https://doi.org/10.1016/j.neunet.2007.04.017

Linkenkaer-Hansen, K., Nikouline, V. V., Palva, J. M., & Ilmoniemi, R. J. (2001). Long-Range Temporal Correlations and Scaling Behavior in Human Brain Oscillations. *The Journal of Neuroscience*, *21*(4), 1370–1377. https://doi.org/10.1523/JNEUROSCI.21-04-01370.2001

Lombardi, F., Shriki, O., Herrmann, H. J., & de Arcangelis, L. (2021). Long-range temporal correlations in the broadband resting state activity of the human brain revealed by neuronal avalanches. *Neurocomputing*, *461*, 657–666. https://doi.org/10.1016/j.neucom.2020.05.126

Manning, J. R., Jacobs, J., Fried, I., & Kahana, M. J. (2009). Broadband Shifts in Local Field Potential Power Spectra Are Correlated with Single-Neuron Spiking in Humans. *Journal of Neuroscience*, *29*(43), 13613–13620. https://doi.org/10.1523/JNEUROSCI.2041-09.2009

Meisel, C., Klaus, A., Kuehn, C., & Plenz, D. (2015). Critical Slowing Down Governs the Transition to Neuron Spiking. *PLOS Computational Biology*, *11*(2), e1004097. https://doi.org/10.1371/journal.pcbi.1004097

Miller, K. J., Sorensen, L. B., Ojemann, J. G., & den Nijs, M. (2009). Power-Law Scaling in the Brain Surface Electric Potential. *PLoS Computational Biology*, *5*(12), e1000609. https://doi.org/10.1371/journal.pcbi.1000609

Moutard, C., Dehaene, S., & Malach, R. (2015). Spontaneous Fluctuations and Non-linear Ignitions: Two Dynamic Faces of Cortical Recurrent Loops. *Neuron*, *88*(1), 194–206. https://doi.org/10.1016/j.neuron.2015.09.018

Mukamel, R., Gelbard, H., Arieli, A., Hasson, U., Fried, I., & Malach, R. (2005). Coupling Between Neuronal Firing, Field Potentials, and fMRI in Human Auditory Cortex. *Science*, *309*(5736), 951–954. https://doi.org/10.1126/science.1110913

Nir, Y., Fisch, L., Mukamel, R., Gelbard-Sagiv, H., Arieli, A., Fried, I., & Malach, R. (2007). Coupling between Neuronal Firing Rate, Gamma LFP, and BOLD fMRI Is Related to Interneuronal Correlations. *Current Biology*, *17*(15), 1275–1285. https://doi.org/10.1016/j.cub.2007.06.066

Nir, Y., Hasson, U., Levy, I., Yeshurun, Y., & Malach, R. (2006). Widespread functional connectivity and fMRI fluctuations in human visual cortex in the absence of visual stimulation. *NeuroImage*, *30*(4), 1313–1324. https://doi.org/10.1016/j.neuroimage.2005.11.018

Nir, Y., Mukamel, R., Dinstein, I., Privman, E., Harel, M., Fisch, L., Gelbard-Sagiv, H., Kipervasser, S., Andelman, F., Neufeld, M. Y., Kramer, U., Arieli, A., Fried, I., & Malach, R. (2008).

Interhemispheric correlations of slow spontaneous neuronal fluctuations revealed in human sensory cortex. *Nature Neuroscience*, *11*(9), 1100–1108. https://doi.org/10.1038/nn.2177

Norman, Y., & Malach, R. (2022). *What can iEEG inform us about mechanisms of spontaneous behavior?* [Preprint]. PsyArXiv. https://doi.org/10.31234/osf.io/94vd5

Norman, Y., Yeagle, E. M., Harel, M., Mehta, A. D., & Malach, R. (2017). Neuronal baseline shifts underlying boundary setting during free recall. *Nature Communications*, *8*(1), 1301. https://doi.org/10.1038/s41467-017-01184-1

O'Byrne, J., & Jerbi, K. (2022). How critical is brain criticality? *Trends in Neurosciences*, *45*(11), 820–837. https://doi.org/10.1016/j.tins.2022.08.007

Palva, J. M., Zhigalov, A., Hirvonen, J., Korhonen, O., Linkenkaer-Hansen, K., & Palva, S. (2013). Neuronal long-range temporal correlations and avalanche dynamics are correlated with behavioral scaling laws. *Proceedings of the National Academy of Sciences*, *110*(9), 3585–3590. https://doi.org/10.1073/pnas.1216855110

Podvalny, E., Noy, N., Harel, M., Bickel, S., Chechik, G., Schroeder, C. E., Mehta, A. D., Tsodyks, M., & Malach, R. (2015). A unifying principle underlying the extracellular field potential spectral responses in the human cortex. *Journal of Neurophysiology*, *114*(1), 505–519. https://doi.org/10.1152/jn.00943.2014

Privman, E., Fisch, L., Neufeld, M. Y., Kramer, U., Kipervasser, S., Andelman, F., Yeshurun, Y., Fried, I., & Malach, R. (2011). Antagonistic Relationship between Gamma Power and Visual Evoked Potentials Revealed in Human Visual Cortex. *Cerebral Cortex*, *21*(3), 616–624. https://doi.org/10.1093/cercor/bhq128

Raichle, M. E. (2011). The Restless Brain. *Brain Connectivity*, *1*(1), 3–12. https://doi.org/10.1089/brain.2011.0019

Ramot, M., Wilf, M., Goldberg, H., Weiss, T., Deouell, L. Y., & Malach, R. (2011). Coupling between spontaneous (resting state) fMRI fluctuations and human oculo-motor activity. *NeuroImage*, *58*(1), 213–225. https://doi.org/10.1016/j.neuroimage.2011.06.015

Raut, R. V., Snyder, A. Z., Mitra, A., Yellin, D., Fujii, N., Malach, R., & Raichle, M. E. (2021). Global waves synchronize the brain's functional systems with fluctuating arousal. *Science Advances*, *7*(30), eabf2709. https://doi.org/10.1126/sciadv.abf2709

Rusakov, D. A., Savtchenko, L. P., & Latham, P. E. (2020). Noisy Synaptic Conductance: Bug or a Feature? *Trends in Neurosciences*, *43*(6), 363–372. https://doi.org/10.1016/j.tins.2020.03.009

Sadaghiani, S., & Kleinschmidt, A. (2013). Functional interactions between intrinsic brain activity and behavior. *NeuroImage*, *80*, 379–386. https://doi.org/10.1016/j.neuroimage.2013.04.100

Scheffer, M., Bascompte, J., Brock, W. A., Brovkin, V., Carpenter, S. R., Dakos, V., Held, H., van Nes, E. H., Rietkerk, M., & Sugihara, G. (2009). Early-warning signals for critical transitions. *Nature*, *461*(7260), 53–59. https://doi.org/10.1038/nature08227

Shew, W. L., & Plenz, D. (2013). The Functional Benefits of Criticality in the Cortex. *The Neuroscientist*, *19*(1), 88–100. https://doi.org/10.1177/1073858412445487

Shew, W. L., Yang, H., Petermann, T., Roy, R., & Plenz, D. (2009). Neuronal Avalanches Imply Maximum Dynamic Range in Cortical Networks at Criticality. *Journal of Neuroscience*, *29*(49), 15595–15600. https://doi.org/10.1523/JNEUROSCI.3864-09.2009

Shriki, O., Alstott, J., Carver, F., Holroyd, T., Henson, R. N. A., Smith, M. L., Coppola, R., Bullmore, E., & Plenz, D. (2013). Neuronal Avalanches in the Resting MEG of the Human Brain. *Journal of Neuroscience*, *33*(16), 7079–7090. https://doi.org/10.1523/JNEUROSCI.4286-12.2013

Shriki, O., Hansel, D., & Sompolinsky, H. (2003). Rate Models for Conductance-Based Cortical Neuronal Networks. *Neural Computation*, *15*(8), 1809–1841. https://doi.org/10.1162/08997660360675053

Shriki, O., & Yellin, D. (2016). Optimal Information Representation and Criticality in an Adaptive Sensory Recurrent Neuronal Network. *PLOS Computational Biology*, *12*(2), e1004698. https://doi.org/10.1371/journal.pcbi.1004698

Smith, S. M., Nichols, T. E., Vidaurre, D., Winkler, A. M., Behrens, T. E. J., Glasser, M. F., Ugurbil, K., Barch, D. M., Van Essen, D. C., & Miller, K. L. (2015). A positive-negative mode of population covariation links brain connectivity, demographics and behavior. *Nature Neuroscience*, *18*(11), 1565–1567. https://doi.org/10.1038/nn.4125

Softky, W., & Koch, C. (1993). The highly irregular firing of cortical cells is inconsistent with temporal integration of random EPSPs. *The Journal of Neuroscience*, *13*(1), 334–350. https://doi.org/10.1523/JNEUROSCI.13-01-00334.1993

Strappini, F., Wilf, M., Karp, O., Goldberg, H., Harel, M., Furman-Haran, E., Golan, T., & Malach, R. (2019). Resting-State Activity in High-Order Visual Areas as a Window into Natural Human Brain Activations. *Cerebral Cortex*, *29*(9), 3618–3635. https://doi.org/10.1093/cercor/bhy242

Sukenik, N., Vinogradov, O., Weinreb, E., Segal, M., Levina, A., & Moses, E. (2021). Neuronal circuits overcome imbalance in excitation and inhibition by adjusting connection numbers. *Proceedings of the National Academy of Sciences*, *118*(12), e2018459118. https://doi.org/10.1073/pnas.2018459118

Tagliazucchi, E., Balenzuela, P., Fraiman, D., & Chialvo, D. R. (2012). Criticality in Large-Scale Brain fMRI Dynamics Unveiled by a Novel Point Process Analysis. *Frontiers in Physiology*, *3*. https://doi.org/10.3389/fphys.2012.00015

Toker, D., Pappas, I., Lendner, J. D., Frohlich, J., Mateos, D. M., Muthukumaraswamy, S., Carhart-Harris, R., Paff, M., Vespa, P. M., Monti, M. M., Sommer, F. T., Knight, R. T., & D'Esposito, M. (2022). Consciousness is supported by near-critical slow cortical electrodynamics. *Proceedings of the National Academy of Sciences*, *119*(7), e2024455119. https://doi.org/10.1073/pnas.2024455119

Wilf, M., Strappini, F., Golan, T., Hahamy, A., Harel, M., & Malach, R. (2015). Spontaneously Emerging Patterns in Human Visual Cortex Reflect Responses to Naturalistic Sensory Stimuli. *Cerebral Cortex*, bhv275. https://doi.org/10.1093/cercor/bhv275

Wilson, H. R., & Cowan, J. D. (1972). Excitatory and Inhibitory Interactions in Localized Populations of Model Neurons. *Biophysical Journal*, *12*(1), 1–24. https://doi.org/10.1016/S0006-3495(72)86068-5

Yarom, Y., & Hounsgaard, J. (2011). Voltage Fluctuations in Neurons: Signal or Noise? *Physiological Reviews*, *91*(3), 917–929. https://doi.org/10.1152/physrev.00019.2010

Yellin, D., Berkovich-Ohana, A., & Malach, R. (2015). Coupling between pupil fluctuations and resting-state fMRI uncovers a slow build-up of antagonistic responses in the human cortex. *NeuroImage*, *106*, 414–427. https://doi.org/10.1016/j.neuroimage.2014.11.034

Yu, S., Yang, H., Shriki, O., & Plenz, D. (2013). Universal organization of resting brain activity at the thermodynamic critical point. *Frontiers in Systems Neuroscience*, *7*. https://doi.org/10.3389/fnsys.2013.00042